EPJ Web of Conferences **273**, 01012 (2022) https://doi.org/10.1051/epjconf/202227301012
JNSPE 2022

XPS chemical state mapping in opto- and microelectronics

Mathieu Frégnaux[1*], *Yoan* Bourlier[1,2], *Bruno* Berini[2], *Yves* Dumont[2], *Damien* Aureau[1]

[1]Institut Lavoisier de Versailles (ILV), CNRS UMR 8180, Université de Versailles Saint-Quentin-en-Yvelines - Université Paris-Saclay, 78000 Versailles, France.
[2]Groupe d'Etude de la Matière Condensée (GEMaC), CNRS UMR 8635, Université de Versailles Saint-Quentin-en-Yvelines - Université Paris-Saclay, 78000 Versailles, France.

Abstract. The strength of XPS imaging lies in its ability to (i) locate small patterns on sample surface, and (ii) inform, with micrometric lateral resolution, about the chemical environment of the elements detected at the surface. In this context, strontium-based perovskites appear to be well-adapted for such photoemission experiments thanks to their tunability and variability. These functional oxides have great potential for emerging opto- and microelectronic applications, especially for transparent conductive oxide. Patterned heterostructure $SrTiO_3/SrVO_3$ was grown by pulsed laser deposition using a shadow mask. This stack was then analysed by XPS mapping in serial acquisition mode. Ti2p and V2p core level imaging clearly highlights the $SrTiO_3$ and $SrVO_3$ domains. The XPS mapping of the Sr3d core level will be extensively discussed: strontium being a common element to both oxides with a very similar chemical environment. Despite a lower contrast in Sr3d images, the two materials are discernible thanks to the topography. In addtion, the use of Sr3d FWHM image is a real asset to evidence the two phases. Finally, data processing by principal component analysis allows us to extract significant spectral information on the strontium atoms.

1 Introduction

X-ray Photoelectron Spectroscopy (XPS) imaging is a real asset to access surface chemical compositions of a few millimeters square patterns. This specific photoemission mode can be useful for (i) confidently locating micrometric objects, or small features at the sample surface (ii) informing on the spatial distribution of the surface constituent elements (elemental mapping) and (iii) locally differentiating between chemical environments. There are two approaches for obtaining XPS images [1]: mapping (serial acquisition) or parallel imaging (parallel acquisition). These different acquisition modes were developed thanks to the reduction of X-ray spot sizes (down to few microns) or the joint use of a lens and a 2D detector, respectively.
Serial acquisition is based on a two-dimensional, rectangular array of small-area XPS [2,3] analyses. The lateral resolution is then determined by the size of the smallest analysis area available (usually few micrometers). Serial acquisition is generally slower compared to parallel acquisition. The data are collected using snapshot (acquired range of energies controlled by the pass energy) at each pixel while only one energy is recorded for parallel acquisition. The maximum size of the image is quite large and is only limited by the range of motion of the specimen stage
Parallel imaging exploits a different way for data acquisition. It images simultaneously the whole field of view for one fixed energy (fixed voltage applied). It requires additional lenses and a two-dimensional detector. The spatial resolution of parallel imaging depends on the spherical aberrations in the lens. Limiting the angular acceptance of the lens can reduce the effect of the aberrations, which improves resolution at the expense of sensitivity. The use of a magnetic immersion lens in the specimen region also reduces aberrations, producing higher sensitivity at a given resolution. Parallel Imaging provides the best resolution and is faster than serial methods for producing an image at a single energy. Spectroscopy from images is possible by collecting a series of images at different energies across the required energy range. A XPS spectrum can be then reconstructed for each pixel in the image.
An alternative approach is parallel imaging using X-ray photoelectron emission microscopy (XPEEM). The lateral resolution of core-level images in the 500 nm range is then achievable [4]. This is a real improvement compared with the capabilities of other lab XPS imaging methods. It uses a bright microfocussed monochromated Al Kα source and a photoelectron emission microscope (PEEM) as entrance lens of a high-transmission, aberration-compensated imaging spectrometer in the form of a double hemispherical analyser. From the instrumental point of view, the main limitation of the technique is the low counting statistics due to the use of a moderately bright millimeter size X-ray spot.
This reduction in lateral resolution makes XPS imaging compatible with the characterization of patterns in a wide range of industrial applications [1] and particularly in the field of micro-optoelectronics: SiGe layers [4], graphene [5], 2D materials [6] transparent conductive oxides [7]. The characteristic dimensions involved for

* Corresponding author: mathieu.fregnaux@uvsq.fr

© The Authors, published by EDP Sciences. This is an open access article distributed under the terms of the Creative Commons Attribution License 4.0 (http://creativecommons.org/licenses/by/4.0/).

such applications, especially thicknesses, require a probe size too small to be characterized with scanning electron microscopy coupled with energy dispersive X-ray spectroscopy (SEM-EDS) for instance. Moreover, the deposition of insulating passivation layers (oxides, nitrides, etc.) makes the use of Auger electron spectroscopy (AES) quite difficult to implement [8]. Under these conditions, despite a lower lateral resolution, XPS imaging with charge neutralization assistance turns out to be a technique of choice.

In contrast to the conventionally held belief of imaging XPS, data acquisition with good signal-to-noise ratio in a reasonable time is possible. Spectra from individual pixel of the image can be plotted or averaged for chemical information. Significant spectral information can be extracted from images, even with low count rate, using mathematical processes [9] such as principal component analysis (PCA).

In this paper, we will focus on XPS imaging in the context of perovskite oxide heterostructure characterization. This class of materials are promising for the emerging field of oxitronics [10] or the development of new transparent conductive oxide [11]. The advantages of serial acquisition that are its ability to produce high resolution, large area XPS images within minutes, will be exploited for this study. For this purpose, a patterned heterostructure $SrTiO_3/SrVO_3$ (STO/SVO) grown by pulsed laser deposition (PLD) on STO substrate will be investigated. Using a shadow mask, micrometer size domains of epitaxial STO with different shapes can be obtained on free SVO.

2 Experimental

SVO and STO targets for PLD were prepared in the GEMaC laboratory from high purity binary oxides powders (SrO/V_2O_5 and SrO/TiO_2) by standard ceramic processing method. The pressed pellet was sintered in air with additional oxygen flow. The “Sr/V” and “Sr/Ti” target metallic ratios were controlled by chemical titration. Single crystal (SurfaceNet GmbH) STO (100) substrates was used for the PLD growth. Depositions of both SVO and STO layers were performed in an ultra-high vacuum chamber with base pressure of 5×10-7 Pa. A shadow mask was applied during the STO deposition to create patterns of various shape and size ranging from millimetres to few ten microns. Targets were ablated using a KrF laser with a wavelength of 248 nm and 20 ns of pulse duration. The laser fluency, the focalization lens position and the laser energy were previously optimized for individual materials. The targeted thicknesses were 20 nm for SVO and 80 nm for STO.

Regular X-ray Photoelectron Spectroscopy (XPS) measurements were carried out using a Thermofisher Scientific Nexsa spectrometer with a monochromatic Al-Kα X-ray source (hν = 1486.6 eV). The detection was performed perpendicularly to the sample surface using a constant analyzer energy (CAE) mode (pass energy 20 eV) and spectra were recorded with a 0.1 eV energy step. The use of low-energy electron and ion flood gun was necessary to perform the analysis. Imaging of the STO/SVO stack was recorded in the “SnapMap” mode with a 50 µm X-ray spot. In such acquisition mode, the micro-focused beam is rastered across the sample by rapid stage movements, yielding an elementary map (O1s, Sr3d, Ti2p and V2p) with a field of view of 3 x 3 mm². Indeed, the stage movement is synchronized with the spectrometer which collects snapshot XPS spectra continuously during rastering. Full spectra are acquired at each pixel with pass energy of 150 eV. Each map required 14 minutes of acquisition time (4 scans). In order to quantify the concentrations of the elements across the images (atomic concentration images), the spectra extracted in each pixel were used to define quantification regions Quantification and image processing including PCA were performed using the Thermofisher Scientific Avantage© software. Chemical compositions and quantitative chemical maps were obtained from the O1s, Sr3d, Ti2p, V2p peak areas after a Shirley type background subtraction and considering “AlThermo1” sensitivity factor library. Concerning PCA data processing, two factors were defined and used. No data scaling was employed but a offset was applied to remove a horizontal baseline at the minimum value of data in each spectrum. Non-negativity fitting was imposed in order to constrain the rotation of factors to produce positive factors.

3 Results and discussion

Fig.1 shows Sr3d spectral regions of both pure STO (black line) and SVO (red line) thin films deposited by PLD on STO substrate. These reference spectra were recorded by regular XPS. In the case of STO substrates, the Sr3d doublet of this reference material is well-defined. The two peaks $Sr3d_{5/2}$ and $Sr3d_{3/2}$ are narrow and separated by 1.76 eV spin orbit splitting. The main peak is centred at 133.4 eV with a full width at half maximum (FWHM) of 0.8 eV. On the contrary, pure SVO thin film exhibits a broad doublet (1.7 eV FWHM) shifted to higher binding energy compared to STO.

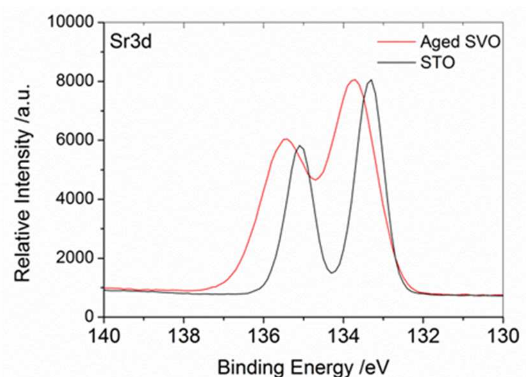

Fig. 1. Sr3d spectral regions of both STO (black) and air-exposed SVO (red) recorded by regular XPS on PLD thin films

It is important to note that this XPS characterization was performed without particular precaution prior analysis. The sample was exposed to air, not store under vacuum or inert atmosphere As SVO surfaces are known to be highly reactive [11,12] and very sensitive to external stimuli [13,14], the obtained Sr3d spectrum in Fig. 1 is the sum of several contributions such as SVO effective

signature but also Sr-rich phases, hydroxides or carbonates. This preliminary work will be essential for the characterization of the STO/SVO heterostructure by serial mapping. The main challenge here will rely in processing the data from the Sr3d core level mapping. Indeed, strontium is common to both oxides with very similar chemical environments, *i.e.* very close in binding energy (see Fig. 1). A robust fitting procedure should be required to extract chemical state mapping of strontium. Fig.2 shows XPS area maps (3 mm x 3 mm) of the STO/SVO stack for Ti2p (a) and V2p (b) spectral regions. The quantitative core level imaging highlights both STO and SVO domains since Ti and V are discriminating elements. The chemical contrast is sharp. This means that no signal from underneath layers is detected. STO patterns cover well the SVO thin film.

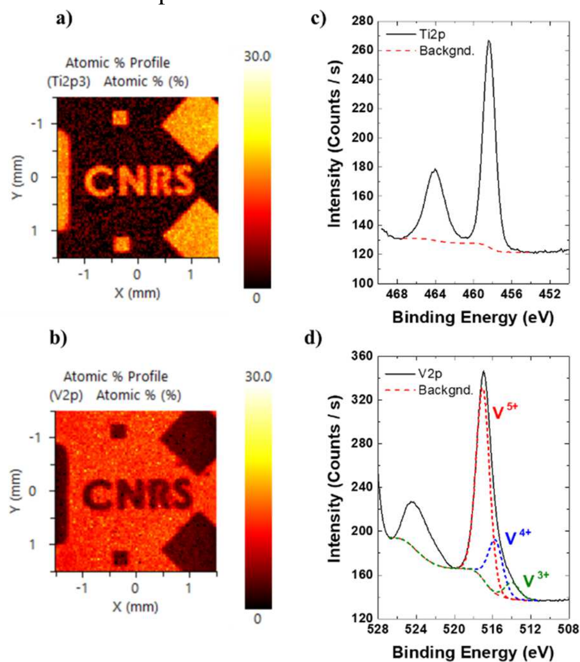

Fig. 2. Quantitative XPS maps (3 mm x 3 mm) of the STO/SVO stack for Ti2p (a) and V2p (b) elements and their corresponding integrated spectrum (c and d). $V2p_{3/2}$ peak is reconstructed to evidence vanadium oxidation states.

Extracted spectrum from Ti2p map (Fig.2 c) is a doublet with $Ti2p_{3/2}$ component at 458.4 eV which is attributed to Ti^{4+}, as expected in STO. Concerning V2p map, the corresponding integrated spectrum (Fig. 2 d) is also a doublet. It is dominated by an intense component at 516.9 eV which corresponds to V^{5+} oxidation state. Small amounts of V^{4+} and V^{3+} are detected at lower binding energy (1.7 and 3.4 eV below) [15]. However, to achieve electrical neutrality in SVO phase, vanadium is expected to be V^{4+}. This discrepancy can be explained by the heterostructure elaboration process. SVO growth was followed by the deposition of STO (under a low oxygen partial pressure). Since vanadium tends to oxidize easily, a small layer with a higher oxidation state V^{5+} on top of vanadate material (likely V_2O_5 phases) has grown during STO deposition. In these conditions, strontium-rich nanostructures can even appear at the surface of SVO. Previous studies [12] demonstrate that vanadium atoms have a high oxidation state (V^{5+}) in these nanostructures.

Fig. 3 a shows quantitative XPS Sr3d map (3 mm x 3 mm) on the same region of interest of the STO/SVO heterostructure. Patterns are no longer discernible since strontium is common to both oxides in similar proportions (20% at.). However, a topographic contrast is visible on the area map (Fig. 3 c) since the STO patterns are deposited on top of the SVO layer providing 80 nm height difference. The corresponding integrated spectrum is presented in Fig. 3 b. It exhibits a broad doublet with a maximum centred at 133.6 eV. Unfortunately, it does not allow us to easily distinguish the respective contributions of STO and SVO.

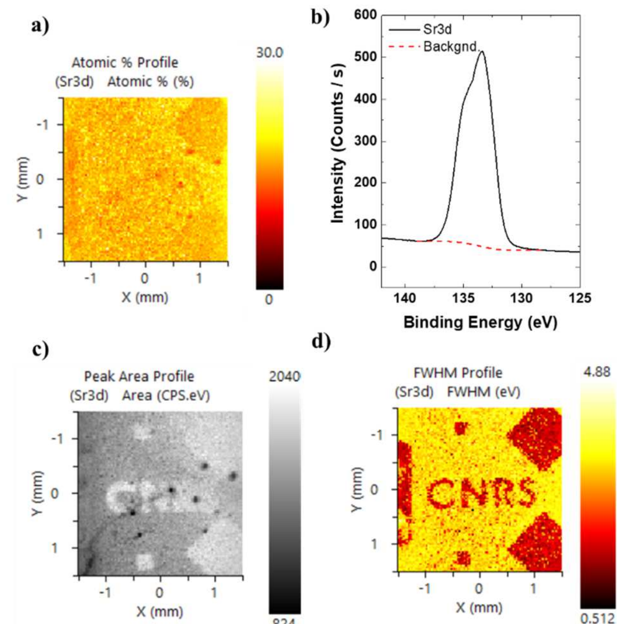

Fig. 3. Quantitative XPS map (3 mm x 3 mm) of the STO/SVO stack for Sr3d (a) and its corresponding integrated spectrum (b). Sr3d area (d) and FWHM (d) maps on the same region of interest.

As demonstrated in reference material (Fig. 1), the positions of Sr3d peak in STO and SVO are close but they present different FWHM. In order to take advantage of this spectroscopic feature, Fig. 3 d presents FWHM map of the STO/SVO stack for Sr3d spectral region. The reasonably good contrast obtained clearly evidences domains with low FWHM associated to STO and others with higher FWHM values attributed to SVO. To extract more information of the Sr3d core level image and get additional knowledge on the chemical environment of the probed strontium atoms in both oxides, a PCA mathematical process was applied. The results obtained are shown in Fig. 4 a-d.

First, two eigenvectors arbitrary named PCA 1 and PCA 2 were sufficient to reconstruct the Sr3d image. They are plotted in Fig. 4 a. Even if these vectors are pure mathematical objects, their shapes satisfactory look like Sr3d doublet. PCA 1 and PCA 2 have a maximum intensity at 133.4 and 132.5 eV, respectively. These positions are really close to the ones measured for $Sr3d_{5/2}$ in STO and SVO, respectively.

Overlayed PCA profiles are presented in Fig 3 (b) while individual PCA 1 and PCA 2 profiles are show in Fig 3 (c) and (d). STO patterns are perfectly reconstructed by PCA 1 profile. The image is similar to the one obtained on Ti2p core level (Fig 2. a), STO discriminating

element. Indeed, Sr3d spectrum recorded in regular XPS on STO patterns (Fig. 4 d) is comparable to the eigenvector PCA 1 (fit with one doublet at 133.4 eV).

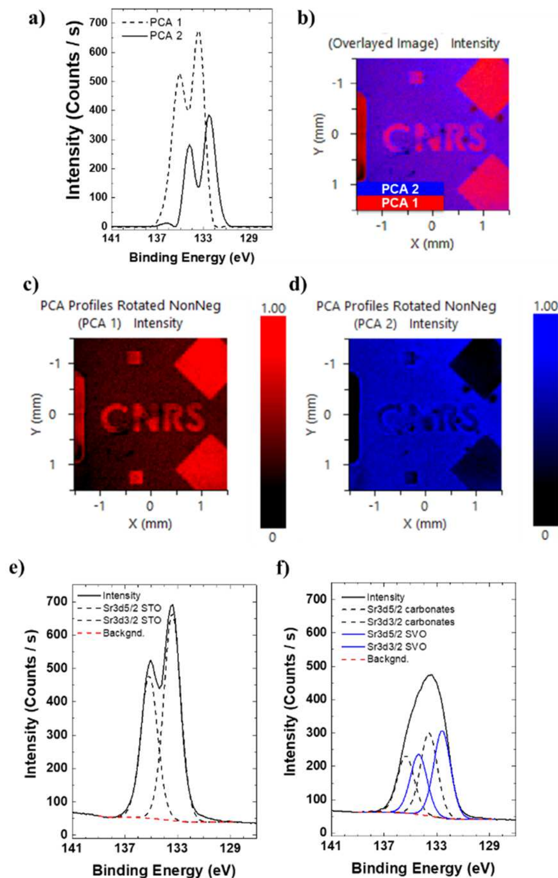

Fig. 4. Sr3d image treatment using PCA mathematical process: (a) eigenvectors considered (PCA 1 and PCA 2), (b) overlayed PCA profiles (c) PCA 1 profile, (d) PCA 2 profile, Sr3d spectrum obtained by regular XPS in STO patterns (e) and free SVO (f)

At first sight, PCA 2 profile would reconstruct the regions with free SVO but it is not the case. A linear combination of 60% PCA 2 with 40% PCA 1 must be considered. This treatment has similarities with the data obtained by regular XPS on free SVO area (Fig. 4 e). Indeed, two doublets are needed to obtain SVO signature: the one at lower binding energy (132.6 eV) is attributed to effective conductive SVO phase while the one at higher binding energy (133.6 eV) corresponds to strontium hydroxydes or strontium carbonates [12].

4 Conclusion

Serial acquisition was used to produce high resolution, large area (3 mm x 3 mm) XPS images of a patterned heterostructure STO/SVO grown by PLD on STO substrate. Using a shadow mask, micrometer size domains of epitaxial STO with different shapes were obtained on free SVO. The Ti2p and V2p area imaging clearly highlights both STO and SVO domains since titanium and vanadium are discriminating elements. The chemical contrast is sharp. This means meaning that no signal from underneath layers is detected and STO patterns entirely cover well the free SVO thin film. Spectroscopy from images confirms the expected oxidation state Ti^{4+} for the titanium in STO and the multiple valence of vanadium dominated by V^{5+} for air-exposed SVO surface. The XPS chemical state mapping of the Sr3d core level is challenging since strontium is a common element to both oxides with a very similar chemical environment. Despite lower contrast in Sr3d images, the two materials are discernible thanks to topography. As the FWHM of air exposed SVO is rather higher than STO one, Sr3d FWHM image is a simple way to evidence the two phases. Moreover, PCA mathematical process was applied on the Sr3d core level image. Two eigenvectors were sufficient to reconstruct the Sr3d image. One of them is enough to reconstruct STO patterns whereas free SVO needs the linear combination of the two eigenvectors. This mathematical processing shows similarities with spectroscopic data.

Acknowledgements:
The authors thank the French Agence Nationale de la Recherche (ANR) in the framework of the POLYNASH project (ANR-17-CE08-0012) for Dr Yoan Bourlier postdoctoral position funding.

References

1. D. J. Morgan, Journal of Electron Spectroscopy and Related Phenomena **231**, 109 (2019).
2. K. Yates and R. H. West, Surface and Interface Analysis **5**, 217 (1983).
3. C. Demanet, Vacuum **37**, 465 (1987).
4. O. Renault, M. Lavayssière, A.Bailly, D. Mariolle et al.., Journal of Electron Spectroscopy and Related Phenomena **171,** 68–71 (2009).
5. A. Tyagi et al., Nanoscale, **14**, 2167-2176 (2022).
6. M. Frégnaux H. Kim, D. Rouchon et al., Surface and Interface Analysis **48**, 465–469 (2016).
7. H. Piao, L. Le Tarte, W.A. Hennessy N. Fairley, Surface and Interface Analysis, **3,** 493-500 (2007).
8. J. Wolstenholme, *Auger Electron Spectroscopy: Practical Application to Materials Analysis and Characterization of Surfaces, Interfaces, and Thin Films* (Momentum Press, 2015).
9. J. Walton and N. Fairley, *The Casa Cookbook Part 2: XPS Image Processing* (Acolyte Science, Knutsford, Cheshire, UK, 2011).
10. M. Coll et al. Applied Surface Science **482**, 1 (2019).
11. A. Boileau, A. Cheikh, A. Fouchet, A. David, C. Labbé, P. Marie, F. Gourbilleau, and U. Lüders, Advanced Optical Materials **7**, 1801516 (2019).
12. Y. Bourlier, M. Frégnaux, B. Bérini, A. Fouchet, Y. Dumont, and D. Aureau, Applied Surface Science **553**, 149536 (2021).
13. Y. Bourlier, M. Frégnaux, B. Bérini, A. Fouchet, Y. Dumont, and D. Aureau, ChemNanoMat **5**, 674 (2019).
14. K. Ridier, D. Aureau, B. Bérini, Y. Dumont, N. Keller, J. Vigneron, A. Etcheberry, B. Domengès, and A. Fouchet, Phys. Rev. B **97**, 035146 (2018).
15. C. Lin, A. Posadas, T. Hadamek, and A. A. Demkov, Phys. Rev. B **92**, 035110 (2015).